In Reference [2] a general method was described for designing reflective N stars for single-mode fiber where $N = M^2$ or $N = 2M^2$. That method is also applicable to designing orthogonal-polarization reflective N stars where $N = M^2$ or $N = 2M^2$. As in Figure 2, an N star, where $N = M^2$, is constructed with M polarization-maintaining transmissive $M \times M$ stars in parallel with one OPFR connected to one output of each $M \times M$ star and with the other outputs of the $M \times M$ stars interconnected with 90° polarization-rotating splices (see Figure 9 of Reference [2]). This design is based on the availability of polarization-maintaining transmissive $M \times M$ stars. For $M = 2^n$, polarization-maintaining transmissive $M \times M$ stars can be constructed by cascading 2×2 PMDCs.

As in Figure 3, reflective N stars, where $N = 2M^2$, are constructed with $2M$ polarization-maintaining transmissive $M \times M$ stars in parallel with M OPHRs. A total of M 90° polarization-rotating splices are used to connect one output port of each pair of adjacent $M \times M$ transmissive stars. And, a total of $M(M-1)/2$ 2×2 PMDCs with a 90° polarization-rotating splice at each input port connect the remaining output ports of the transmissive stars (see Figure 13 of Reference [2]).

III. CONCLUSIONS

Multipath-free orthogonal-polarization reflective N-star networks are proposed where $N = M^2$ and $N = 2M^2$ for $M = 2^n$. These networks use polarization-maintaining fiber and are constructed with $M \times M$ transmissive polarization-maintaining directional couplers, 90° polarization-rotating splices, orthogonal-polarization full reflectors, and orthogonal-polarization half reflectors. The all-fiber design is theoretically lossless and does not require optical isolation. In an actual network the amount of light that is directed toward the transmitters depends on the polarization isolation of the PBS and PMDC, polarization coupling in the fiber, and splice alignment. Ideally, the isolation can be > 25 dB [5, 6, 8, 10]. This is much lower than the 3-dB isolation of a reflective star using single-mode fiber and nonpolarization-preserving fiber directional couplers.

REFERENCES

1. M. E. Marhic, "Hierarchic and Combinatorial Star Couplers," *Opt. Lett.*, Vol. 9, 1984, pp. 368–370.
2. A. A. M. Saleh and H. Kogelnik, "Reflective Single-Mode Fiber-Optic Passive Star Couplers," *J. Lightwave Technol.*, Vol. 6, 1988, pp. 392–397.
3. A. S. Siddiqui and J. Zhou, "Two-Channel Optical Fiber Transmission using Polarization Division Multiplexing," *J. Opt. Commun.*, Vol. 12, 1991, pp. 47–49.
4. Y. Sasaki, K. Tajima, and I. Yokohama, "Bidirectional Optical Transmission Using Polarised Light Waves," *Electron. Lett.*, Vol. 23, 1987, pp. 692–694.
5. J. Noda, K. Okamoto, and Y. Sasaki, "Polarization-Maintaining Fibers and their Applications," *J. Lightwave Technol.*, Vol. 4, 1986, pp. 1071–1089.
6. M. Eisenmann and E. Weidel, "Single-Mode Fused Biconical Coupler Optimized for Polarization Beamsplitting," *J. Lightwave Technol.*, Vol. 9, 1991, pp. 853–858.
7. T. Morioka, H. Takara, K. Mori, and M. Saruwatari, "Ultrafast Reflective Optical Kerr Demultiplexer Using Polarisation Rotation Mirror," *Electron. Lett.*, Vol. 28, 1992, pp. 521–522.
8. J. Noda, N. Shibata, T. Edahiro, and T. Sasaki, "Splicing of Single Polarization-Maintaining Fibers," *J. Lightwave Technol.*, Vol. 1, 1983, pp. 61–66.
9. M. Martinelli, "A Universal Compensator for Polarization Changes Induced by Birefringence on a Retracing Beam," *Opt. Commun.*, Vol. 72, 1989, pp. 341–344.
10. Y. Anjan and S. Habbel, "Environmental Performance of Fused PM Fiber Couplers for Fiber Gyro Application," *IEEE Photon Technol. Lett.*, Vol. PTL-3, 1991, pp. 578–580.

Received 3-29-94

Microwave and Optical Technology Letters, 7/13, 597–599
Published by John Wiley & Sons, Inc.

A 3D PERFECTLY MATCHED MEDIUM FROM MODIFIED MAXWELL'S EQUATIONS WITH STRETCHED COORDINATES

Weng Cho Chew and William H. Weedon
Electromagnetics Laboratory
Department of Electrical and Computer Engineering
University of Illinois
Urbana, Illinois 61801

KEY TERMS

Maxwell's equations, coordinate stretching, perfectly matched layer, finite-difference time domain, massively parallel computer

ABSTRACT

A modified set of Maxwell's equations is presented that includes complex coordinate stretching along the three Cartesian coordinates. The added degrees of freedom in the modified Maxwell's equations allow the specification of absorbing boundaries with zero reflection at all angles of incidence and all frequencies. The modified equations are also related to the perfectly matched layer that was presented recently for 2D wave propagation. Absorbing-material boundary conditions are of particular interest for finite-difference time-domain (FDTD) computations on a single-instruction multiple-data (SIMD) massively parallel supercomputer. A 3D FDTD algorithm has been developed on a connection machine CM-5 based on the modified Maxwell's equations and simulation results are presented to validate the approach. © *1994 John Wiley & Sons, Inc.*

1. INTRODUCTION

The finite-difference time-domain method [1, 2] is widely regarded as one of the most popular computational electromagnetics algorithms. Although FDTD is conceptually very simple and relatively easy to program, the method is actually quite efficient, because it involves $O(N^{1.5})$ computational complexity in 2D and $O(N^{1.33})$ computational complexity in 3D [3]. In fact, FDTD can be considered an optimal algorithm, because $O(N^\alpha)$ numbers are produced in $O(N^\alpha)$ operations.

FDTD is also ideally suited for implementation on a single-instruction multiple-data (SIMD) massively parallel computer. The reason is that the stencil operations that must be computed at each node of the space grid involve only nearest-neighbor interactions and may be implemented at a minimum communication cost [4]. A major challenge, however, is in implementing absorbing boundary conditions (ABCs) at the edges of the FDTD grid. On scalar and vector computers, these boundary conditions are typically computed using methods such as the Engquist-Majda [5], Mur [6], Liao, Wong, Yang and Yuan [7], or Higdon [8] ABC. However,

these methods are not ideal for parallel supercomputers, because they all involve communication with many elements normal to the grid boundary. Such communication can easily surpass the time spent computing core FDTD operations in the grid interior, especially for higher-order boundary conditions, and hence can become a bottleneck in the FDTD code. Also, they do not allow for SIMD operation on a parallel machine without the use of masking.

An alternate method of implementing an ABC is to use a conventional absorbing material boundary [4, 9–14]. For SIMD parallel computation, these methods have the advantage that the ABC may be implemented with the same FDTD stencil operation as the interior nodes by modifying the conductivity material parameter at the edge of the FDTD grid. The disadvantage is that the reflection coefficient at the absorbing border is zero only at normal incidence and is both angle and frequency dependent. Consequently, the absorbing material border region must be made quite large—typically 20–100 grid points along each edge in order to minimize reflections.

Recently, Berenger [15] suggested a more general method of implementing an absorbing material boundary condition. Berenger proposed a procedure for 2D wave propagation whereby Maxwell's equations are generalized and added degrees of freedom are introduced. The added degrees of freedom allow the specification of absorbing borders with zero reflection coefficient at all angles of incidence and all frequencies. Moreover, the generalized Maxwell's equations reduce to the familiar Maxwell's equations as a special case and hence the same generalized equations can be used to propagate fields in both the interior and absorbing regions. Although the interface between the interior region and the absorbing boundary is reflectionless, there is still a reflection from the edge of the grid. The advantage of using Berenger's procedure is that much larger conductivity values may be specified in the absorbing region, leading to a drastic reduction in the number of grid points required for the absorbing boundary.

In the present article a formulation similar to the Berenger idea is derived for 3D wave propagation from first principles using a coordinate stretching approach. The advantage of the new method for SIMD parallel computation is stressed. The method is validated with 3D FDTD numerical computations on a Thinking Machines Corporation Connection Machine CM-5.

2. MODIFIED MAXWELL'S EQUATIONS

For a general medium, we define the modified Maxwell's equations in the frequency domain, assuming $e^{-i\omega t}$ time dependence, as

$$\nabla_e \times \mathbf{E} = i\omega\mu\mathbf{H}, \tag{1}$$

$$\nabla_h \times \mathbf{H} = -i\omega\epsilon\mathbf{E}, \tag{2}$$

$$\nabla_h \cdot \epsilon\mathbf{E} = \rho, \tag{3}$$

$$\nabla_e \cdot \mu\mathbf{H} = 0, \tag{4}$$

where

$$\nabla_e = \hat{x}\frac{1}{e_x}\frac{\partial}{\partial x} + \hat{y}\frac{1}{e_y}\frac{\partial}{\partial y} + \hat{z}\frac{1}{e_z}\frac{\partial}{\partial z} \tag{5}$$

$$\nabla_h = \hat{x}\frac{1}{h_x}\frac{\partial}{\partial x} + \hat{y}\frac{1}{h_y}\frac{\partial}{\partial y} + \hat{z}\frac{1}{h_z}\frac{\partial}{\partial z}. \tag{6}$$

In the above, e_i, h_i, $i = x, y, z$ are coordinate-stretching variables that stretch the x, y, z coordinates for ∇_e and ∇_h. It shall be shown later that when e_i and h_i are complex numbers, the medium can be lossy. Note that (3) and (4) are derivable from (1) and (2). A general plane-wave solution to Eqs. (1)–(4) has the form

$$\mathbf{E} = \mathbf{E}_0 e^{i\mathbf{k}\cdot\mathbf{r}} \tag{7}$$

and

$$\mathbf{H} = \mathbf{H}_0 e^{i\mathbf{k}\cdot\mathbf{r}}, \tag{8}$$

where $\mathbf{k} = \hat{x}k_x + \hat{y}k_y + \hat{z}k_z$. Substituting Eqs. (7) and (8) into Eqs. (1) and (2) above gives

$$\mathbf{k}_e \times \mathbf{E} = \omega\mu\mathbf{H}, \tag{9}$$

$$\mathbf{k}_h \times \mathbf{H} = -\omega\epsilon\mathbf{E}, \tag{10}$$

where

$$\mathbf{k}_e = \hat{x}\frac{k_x}{e_x} + \hat{y}\frac{k_y}{e_y} + \hat{z}\frac{k_z}{e_z}$$

and

$$\mathbf{k}_h = \hat{x}\frac{k_x}{h_x} + \hat{y}\frac{k_y}{h_y} + \hat{z}\frac{k_z}{h_z}.$$

Combining the above, we have

$$\begin{aligned} -\omega^2\mu\epsilon\mathbf{H} &= \mathbf{k}_e \times \mathbf{k}_h \times \mathbf{H} \\ &= \mathbf{k}_h(\mathbf{k}_e \cdot \mathbf{H}) - (\mathbf{k}_e \cdot \mathbf{k}_h)\mathbf{H}. \end{aligned} \tag{11}$$

But from Eq. (9), $\mathbf{k}_e \cdot \mathbf{H} = 0$ for a homogeneous medium. This gives the dispersion relation

$$\omega^2\mu\epsilon = \mathbf{k}_e \cdot \mathbf{k}_h \tag{12}$$

or

$$\kappa^2 = \frac{1}{e_x h_x}k_x^2 + \frac{1}{e_y h_y}k_y^2 + \frac{1}{e_z h_z}k_z^2 \tag{13}$$

where $\kappa^2 = \omega^2\mu\epsilon$. Equation (13) is the equation of an ellipsoid in 3D and is satisfied by

$$k_x = \kappa\sqrt{e_x h_x}\sin\theta\cos\phi, \tag{14}$$

$$k_y = \kappa\sqrt{e_y h_y}\sin\theta\sin\phi, \tag{15}$$

and

$$k_z = \kappa\sqrt{e_z h_z}\cos\theta. \tag{16}$$

Note that when e_i, h_i, $i = x, y, z$ are complex, the waves in the x, y, and z directions are attenuative and can be independently controlled. Under the matching condition, $e_x = h_x$, $e_y = h_y$, and $e_z = h_z$, we have $|\mathbf{k}_e|^2 = |\mathbf{k}_h|^2 = \kappa^2$. The wave impedance is then given by

$$\eta = \frac{|\mathbf{E}|}{|\mathbf{H}|} = \frac{|\mathbf{k}_h|}{\omega\epsilon} = \sqrt{\frac{\mu}{\epsilon}}, \tag{17}$$

irrespective of the values for e_i, $i = x, y, z$ and the direction of propagation.

3. SINGLE-INTERFACE PROBLEM

Assume that a plane wave is obliquely incident on the interface $z = 0$ in Figure 1. Furthermore, we may assume that the plane wave is of arbitrary polarization. The incident field may be decomposed into a sum of two components, one with electric field transverse to z (TE^z) and the other with magnetic field transverse to z (TM^z). We will examine these two components individually.

In the TE^z case, we let the incident field in region 1 be given as

$$\mathbf{E}_i = \mathbf{E}_0 e^{i\mathbf{k}_i \cdot \mathbf{r}}. \tag{18}$$

In the above, $\mathbf{k}_{hi} \cdot \mathbf{E}_0 = 0$, and $\mathbf{E}_0$ is in the xy plane. Similarly, we define the reflected field in region 1 as

$$\mathbf{E}_r = R^{\mathrm{TE}} \mathbf{E}_{0r} e^{i\mathbf{k}_r \cdot \mathbf{r}}, \tag{19}$$

and the transmitted field in region 2 as

$$\mathbf{E}_t = T^{\mathrm{TE}} \mathbf{E}_{0t} e^{i\mathbf{k}_t \cdot \mathbf{r}}. \tag{20}$$

Phase matching requires that $k_{ix} = k_{rx} = k_{tx}$ and $k_{iy} = k_{ry} = k_{ty}$. Hence, we can define $\mathbf{E}_{0r} = \mathbf{E}_{0t} = \mathbf{E}_0$ because they all point in the same direction. Applying the boundary condition that the tangential electric field must be continuous across the plane $z = 0$,[1] we have

$$1 + R^{\mathrm{TE}} = T^{\mathrm{TE}}. \tag{21}$$

The magnetic field may be determined using Eq. (9) for regions 1 and 2 as

$$\mathbf{H}_1 = \frac{\mathbf{k}_{ie} \times \mathbf{E}_0}{\omega \mu_1} e^{i\mathbf{k}_i \cdot \mathbf{r}} + R^{\mathrm{TE}} \frac{\mathbf{k}_{re} \times \mathbf{E}_0}{\omega \mu_1} e^{i\mathbf{k}_r \cdot \mathbf{r}} \tag{22}$$

and

$$\mathbf{H}_2 = T^{\mathrm{TE}} \frac{\mathbf{k}_{te} \times \mathbf{E}_0}{\omega \mu_2} e^{i\mathbf{k}_t \cdot \mathbf{r}}, \tag{23}$$

where

$$\mathbf{k}_{ie} = \hat{x} \frac{k_{ix}}{e_x} + \hat{y} \frac{k_{iy}}{e_y} + \hat{z} \frac{k_{iz}}{e_z}$$

and similarly for $\mathbf{k}_{re}$ and $\mathbf{k}_{te}$. We also define $k_{1z} = k_{iz}$, $k_{2z} = k_{tz}$ and note that $k_{rz} = -k_{1z}$. Then equating the tangential components of Eqs. (22) and (23), we have

$$k_{1z} e_{2z} \mu_2 [1 - R^{\mathrm{TE}}] = T^{\mathrm{TE}} k_{2z} e_{1z} \mu_1. \tag{24}$$

Combining Eqs. (21) and (24), we have

$$R^{\mathrm{TE}} = \frac{k_{1z} e_{2z} \mu_2 - k_{2z} e_{1z} \mu_1}{k_{1z} e_{2z} \mu_2 + k_{2z} e_{1z} \mu_1} \tag{25}$$

[1] This boundary condition follows from the modified Maxwell's equation (1).

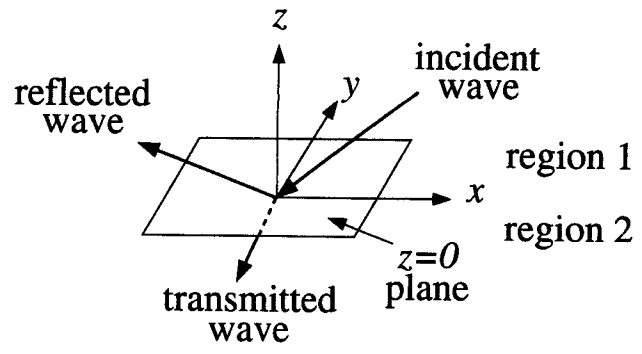

Figure 1 Plane wave with arbitrary polarization incident on the plane $z = 0$

and

$$T^{\mathrm{TE}} = \frac{2k_{1z} e_{2z} \mu_2}{k_{1z} e_{2z} \mu_2 + k_{2z} e_{1z} \mu_1}. \tag{26}$$

Applying a similar procedure to the TM^z component, we have

$$R^{\mathrm{TM}} = \frac{k_{1z} h_{2z} \epsilon_2 - k_{2z} h_{1z} \epsilon_1}{k_{1z} h_{2z} \epsilon_2 + k_{2z} h_{1z} \epsilon_1} \tag{27}$$

and

$$T^{\mathrm{TM}} = \frac{2k_{1z} h_{2z} \epsilon_2}{k_{1z} h_{2z} \epsilon_2 + k_{2z} h_{1z} \epsilon_1}. \tag{28}$$

4. A PERFECTLY MATCHED INTERFACE

The phase matching condition requires that $k_{1x} = k_{2x}$ and $k_{1y} = k_{2y}$, or

$$\kappa_1 \sqrt{e_{1x} h_{1x}} \sin\theta_1 \cos\phi_1 = \kappa_2 \sqrt{e_{2x} h_{2x}} \sin\theta_2 \cos\phi_2 \tag{29}$$

and

$$\kappa_1 \sqrt{e_{1y} h_{1y}} \sin\theta_1 \sin\phi_1 = \kappa_2 \sqrt{e_{2y} h_{2y}} \sin\theta_2 \sin\phi_2, \tag{30}$$

where $\kappa_1 = \omega\sqrt{\mu_1 \epsilon_1}$ and $\kappa_2 = \omega\sqrt{\mu_2 \epsilon_2}$. For a perfectly matched medium, we choose $\epsilon_1 = \epsilon_2$, $\mu_1 = \mu_2$, $e_x = h_x$ and $e_y = h_y$. Equations (29) and (30) become

$$e_{1x} \sin\theta_1 \cos\phi_1 = e_{2x} \sin\theta_2 \cos\phi_2 \tag{31}$$

and

$$e_{1y} \sin\theta_1 \sin\phi_1 = e_{2y} \sin\theta_2 \sin\phi_2. \tag{32}$$

If we now choose $e_{1x} = e_{2x}$ and $e_{1y} = e_{2y}$, then $\theta_1 = \theta_2$, $\phi_1 = \phi_2$ and we can show that both $R^{\mathrm{TE}} = 0$ and $R^{\mathrm{TM}} = 0$ for all angles of incidence and all frequencies.

If region 1 is a vacuum, then $\mu = \mu_0$, $\epsilon = \epsilon_0$, and

$$(e_{1x}, e_{1y}, e_{1z}, h_{1x}, h_{1y}, h_{1z}) = (1, 1, 1, 1, 1, 1). \tag{33}$$

In order to have a lossy region 2 with no reflections at the region 1/region 2 interface, we choose

$$(e_{2x}, e_{2y}, e_{2z}, h_{2x}, h_{2y}, h_{2z}) = (1, 1, s_2, 1, 1, s_2), \tag{34}$$

where s_2 is a complex number. In this case,

$$k_{1x} = k_{2x} = \kappa_0 \sin\theta\cos\phi, \tag{35}$$

$$k_{1y} = k_{2y} = \kappa_0 \sin\theta\sin\phi, \tag{36}$$

$$k_{1z} = \kappa_0 \cos\theta, \tag{37}$$

$$k_{2z} = \kappa_0 s_2 \cos\theta, \tag{38}$$

where $\kappa_0 = \omega\sqrt{\mu_0\epsilon_0}$. If $s_2 = s_2' + is_2''$, the wave will attenuate in the z direction. This kind of interface is useful for building material ABCs in a FDTD simulation.

5. MODIFIED EQUATIONS IN THE TIME DOMAIN

For the general case of a matched medium, we let $e_x = h_x = s_x$, $e_y = h_y = s_y$ and $e_z = h_z = s_z$. Then, $\nabla_e = \nabla_h = \hat{x}\frac{1}{s_x}\frac{\partial}{\partial x} + \hat{y}\frac{1}{s_y}\frac{\partial}{\partial y} + \hat{z}\frac{1}{s_z}\frac{\partial}{\partial z}$. In Eq. (1), we write the curl as

$$\nabla_e \times \mathbf{E} = \frac{1}{s_x}\frac{\partial}{\partial x}\hat{x}\times\mathbf{E} + \frac{1}{s_y}\frac{\partial}{\partial y}\hat{y}\times\mathbf{E} + \frac{1}{s_z}\frac{\partial}{\partial z}\hat{z}\times\mathbf{E}. \tag{39}$$

Then, defining $\mathbf{H}_{s_x}$, $\mathbf{H}_{s_y}$, and $\mathbf{H}_{s_z}$ in terms of the components of Eq. (39), we let

$$i\omega\mu\mathbf{H}_{s_x} = \frac{1}{s_x}\frac{\partial}{\partial x}\hat{x}\times\mathbf{E}, \tag{40}$$

$$i\omega\mu\mathbf{H}_{s_y} = \frac{1}{s_y}\frac{\partial}{\partial y}\hat{y}\times\mathbf{E} \tag{41}$$

and

$$i\omega\mu\mathbf{H}_{s_z} = \frac{1}{s_z}\frac{\partial}{\partial z}\hat{z}\times\mathbf{E} \tag{42}$$

where $\mathbf{H} = \mathbf{H}_{s_x} + \mathbf{H}_{s_y} + \mathbf{H}_{s_z}$. Similarly, we can write Eq. (2) as

$$-i\omega\epsilon\mathbf{E}_{s_x} = \frac{1}{s_x}\frac{\partial}{\partial x}\hat{x}\times\mathbf{H}, \tag{43}$$

$$-i\omega\epsilon\mathbf{E}_{s_y} = \frac{1}{s_y}\frac{\partial}{\partial y}\hat{y}\times\mathbf{H}, \tag{44}$$

and

$$-i\omega\epsilon\mathbf{E}_{s_z} = \frac{1}{s_z}\frac{\partial}{\partial z}\hat{z}\times\mathbf{H}. \tag{45}$$

where $\mathbf{E} = \mathbf{E}_{s_x} + \mathbf{E}_{s_y} + \mathbf{E}_{s_z}$. Note that $\mathbf{H}_{s_i}$, $\mathbf{E}_{s_i}$, $i = x, y, z$ are two-component vectors.

We now let $s_x = 1 + i\sigma_x/\omega\epsilon$, $s_y = 1 + i\sigma_y/\omega\epsilon$, and $s_z = 1 + i\sigma_z/\omega\epsilon$. Writing Eqs. (40)–(42) and (43)–(45) in the time domain, we have

$$\mu\frac{\partial\mathbf{H}_{s_x}}{\partial t} + \frac{\sigma_x\mu}{\epsilon}\mathbf{H}_{s_x} = -\frac{\partial}{\partial x}\hat{x}\times\mathbf{E}, \tag{46}$$

$$\mu\frac{\partial\mathbf{H}_{s_y}}{\partial t} + \frac{\sigma_y\mu}{\epsilon}\mathbf{H}_{s_y} = -\frac{\partial}{\partial y}\hat{y}\times\mathbf{E}, \tag{47}$$

$$\mu\frac{\partial\mathbf{H}_{s_z}}{\partial t} + \frac{\sigma_z\mu}{\epsilon}\mathbf{H}_{s_z} = -\frac{\partial}{\partial z}\hat{z}\times\mathbf{E}, \tag{48}$$

and

$$\epsilon\frac{\partial\mathbf{E}_{s_x}}{\partial t} + \sigma_x\mathbf{E}_{s_x} = \frac{\partial}{\partial x}\hat{x}\times\mathbf{H} \tag{49}$$

$$\epsilon\frac{\partial\mathbf{E}_{s_y}}{\partial t} + \sigma_y\mathbf{E}_{s_y} = \frac{\partial}{\partial y}\hat{y}\times\mathbf{H}, \tag{50}$$

$$\epsilon\frac{\partial\mathbf{E}_{s_z}}{\partial t} + \sigma_z\mathbf{E}_{s_z} = \frac{\partial}{\partial z}\hat{z}\times\mathbf{H}. \tag{51}$$

Equations (46)–(51) describe 3D wave propagation in a perfectly matched medium. The wave-propagation phenomenon described by these equations is very similar to that described by Maxwell's equations with the exception that attenuation may be controlled through the σ_x, σ_y and σ_z variables. The FDTD implementation of these equations on a Yee FDTD grid is straightforward. Absorbing boundaries at the edges of the simulation region may be created by choosing appropriate values of σ_x, σ_y, and σ_z. Equations (46)–(51) may be seen to include Berenger's equations [15] as a subset for the 2D TE or TM case.

The above equations involve 12 components of electromagnetic fields. For a free-space/lossy-medium interface, a scheme may be devised using only 10 field components for the 3D case, and only 3 components for the 2D case. However, this is achieved at the loss of SIMD operation on a parallel machine.

6. COMPUTER SIMULATION RESULTS

In order to demonstrate the new method, a 3D orthogonal grid FDTD algorithm was developed based on Eqs. (46)–(51). The FDTD algorithm was implemented as a SIMD code on the Thinking Machines Corporation Connection Machine CM-5. The algorithm operates very efficiently on the CM-5 because the FDTD stencil operations that need to be computed at each node involve only nearest-neighbor interactions. The communication operations resulting from the nearest-neighbor interactions are at a minimum cost, since the neighboring processors are for the most part at the bottom of the fat-tree communication network, where communication bandwidth is maximum.

To validate our 3D FDTD algorithm, we solved a simple problem of computing the field radiated from an infinitesimal electric dipole in free space. An analytic solution was also computed in the frequency domain for many excitation frequencies. The frequency-domain solution was then multiplied by the spectrum of FDTD source pulse and inverse Fourier transform to yield a time-domain analytic solution for comparison with the FDTD solution.

The FDTD solution was solved in a cubic region of dimension $(N_x, N_y, N_z) = (128, 128, 32)$ grid points. The grid parameters chosen were $\Delta x = \Delta y = \Delta z = 2.5$ mm, $\Delta t = 4.5$ ps and $N_t = 512$ time steps were computed.

The infinitesimal electric dipole was simulated by exciting the E_y field in a single grid cell with the source pulse

$$J_y(t) = \frac{1}{\Delta x\,\Delta y\,\Delta z}[4(t/\tau)^3 - (t/\tau)^4]e^{-t/\tau}, \tag{52}$$

where $\tau = 1/4\pi f_0$ and a value of $f_0 = 1.0$ GHz was chosen. The dipole source was located at grid location $(n_x, n_y, n_z) = (91, 64, 16)$. The E_x and E_y fields were obtained by sampling the fields at grid location $(n_x, n_y, n_z) = (37, 91, 16)$.

The absorbing boundaries used for the FDTD simulation consisted of planar layers of thickness eight grid points on all surfaces. Along the borders parallel to the x axis, the value of σ_x was specified, and σ_y and σ_z were specified on the borders parallel to the y and z axes, respectively. The conductivity values were chosen with a parabolic taper decreasing from the maximum value toward the center of the grid such that the reflection coefficient at normal incidence was $R_0 = 0.0001$.

The E_x field computed using both the analytic formulation and the FDTD algorithm are overlaid in Figure 2. The curves due to the analytic and numerical solutions are barely distinguishable, indicating excellent agreement. Similarly, the E_y field due to the analytic and numerical solutions are overlaid in Figure 3. Again, we see excellent agreement. Any difference between the analytic and numerical solutions in Figures 2 and 3 may be attributed to modeling errors such as the finite size of the dipole source and the discrete approximation of Maxwell's equations in addition to reflections due to imperfections in the absorbing boundaries.

The CM-5 machine used to solve the FDTD problem is located at the National Center for Supercomputing Applications (NCSA) at the University of Illinois. The program was written in CM Fortran and compiled using CMF version 2.1. The CM-5 at the NCSA has 512 nodes with vector units. CPU times were determined by running the problem on 32-, 64-, 128-, and 256-node partitions. For this problem, a total of 0.5 million unknown field quantities (128 × 128 × 32 grid) were determined for 512 time steps. The CPU times are shown in Table 1.

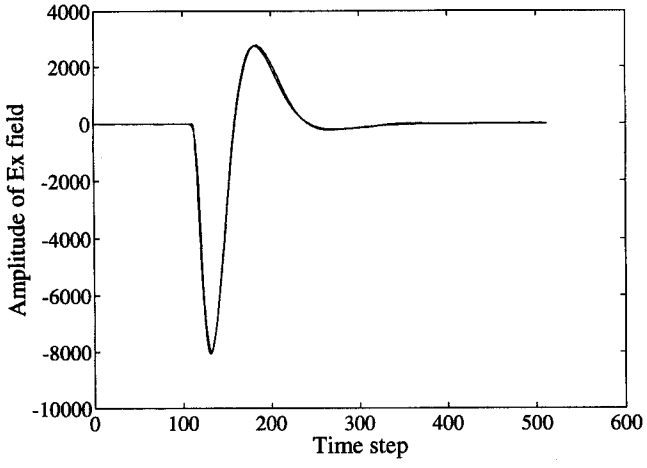

Figure 2 Analytic and numerical FDTD solution overlaid for the E_x field resulting from an infinitesimal electric dipole

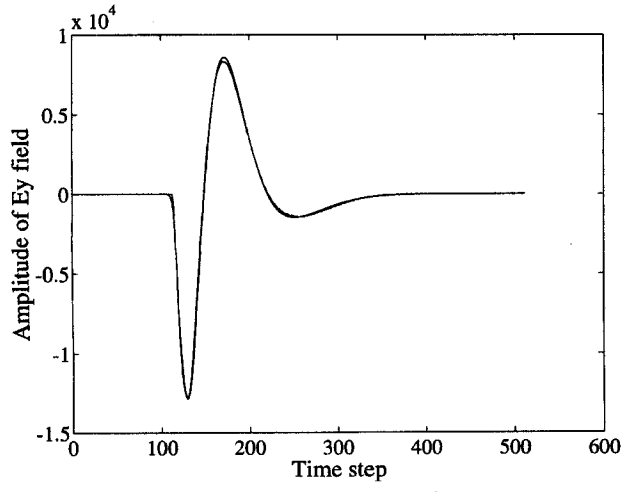

Figure 3 Analytic and numerical FDTD solution overlaid for the E_y field resulting from an infinitesimal electric dipole

TABLE 1. CPU times for FDTD Problem on CM-5

Nodes	CPU sec (Run 1, Run 2, Run 3; Avg.)
32	50.5, 50.2, 50.6; 50.4
64	29.9, 30.0, 30.0; 30.0
128	17.9, 18.4, 18.4; 18.2
256	12.4, 13.2, 12.7; 12.8

7. CONCLUSIONS

A modified set of Maxwell's equations have been introduced using complex coordinate stretching factors along the three Cartesian coordinate axes. This modification introduces additional degrees of freedom in Maxwell's equations such that absorbing boundaries may be specified with zero reflection coefficient at all frequencies and all angles of incidence. The formulation was shown to be related to the perfectly matched layer that was recently derived by Berenger for 2D wave propagation. A 3D FDTD algorithm was developed from the modified Maxwell's equations that use the reflectionless absorbing interface property to implement radiation boundary conditions at the edges of the FDTD grid. The accuracy of the algorithm was validated by computing the field radiated from an infinitesimal electric dipole and comparing against a known analytical expression. The FDTD algorithm was implemented on the Connection Machine CM-5 and timing results were presented. This breakthrough in absorbing material boundary conditions allows EM scattering to be computed very efficiently on SIMD parallel computers.

ACKNOWLEDGMENT

The authors wish to thank J.-P. Berenger for sending us a preprint of his work and to A. Taflove for bringing to our attention J.-P. Berenger's work. This work is supported by the Office of Naval Research under Grant No. N000-14-89-J1286, the Army Research Office under Contract No. DAAL03-91-G-0339, the National Science Foundation under Grant No. NSF-ECS-92-24466, and NASA under Grant No. NASA-NAG-2-871. Computer time is provided by the National Center for Supercomputer Applications at the University of Illinois, Urbana-Champaign.

REFERENCES

1. K. S. Yee, "Numerical Solution of Initial Boundary Value Problems Involving Maxwell's Equations in Isotropic Media," *IEEE Trans. Antennas Propagat.*, Vol. AP-14, 1966, pp. 302–307.
2. A. Taflove, "Review of the Formulation and Applications of the Finite-Difference Time-Domain Method for Numerical Modeling of Electromagnetic Wave Interactions with Arbitrary Structures," *Wave Motion*, Vol. 10, pp. 547–582, 1988.
3. W. C. Chew, *Waves and Fields in Inhomogeneous Media*, Van Nostrand, New York, 1990.
4. W. H. Weedon, W. C. Chew, and C. M. Rappaport, "Computationally Efficient FDTD Simulation of Open-Region Scattering Problems on the Connection Machine CM-5," in *IEEE Antennas and Propagation Society International Symposium Digest*, Seattle, WA, June 19–24, 1994.

5. B. Engquist and A. Majda, "Absorbing Boundary Conditions for the Numerical Simulation of Waves," *Math. Comput.*, Vol. 31, 1977, pp. 629–651.
6. G. Mur, "Absorbing Boundary Conditions for the Finite-Difference Approximation of the Time-Domain Electromagnetic Field Equations," *IEEE Trans. Electromagn. Compat.*, Vol. EMC-23, 1981, pp. 377–382.
7. Z. P. Liao, H. L. Wong, B. P. Yang, and Y. F. Yuan, "A Transmitting Boundary for Transient Wave Analysis," *Sci. Sin. Ser. A*, Vol. 27, No. 10, 1984, pp. 1063–1076.
8. R. L. Higdon, "Numerical Absorbing Boundary Conditions for the Wave Equation," *Math. Comput.*, Vol. 49, 1987, pp. 65–90.
9. I. Katz, D. Parks, A. Wilson, M. Rotenberg, and J. Harren, "Non-Reflective Free Space Boundary Conditions for SGEMP Codes," *Syst., Sci. Software*, Vol. SSS-R-76-2934, 1976.
10. R. Holland and J. W. Williams, "Total-Field versus Scattered-Field Finite-Difference Codes: A Comparative Assessment," *IEEE Trans. Nucl. Sci.*, Vol. NS-30, 1983, pp. 4583–4588.
11. J.-P. Berenger, in *Actes du Colloque CEM*, (Tregastel, France), 1983.
12. C. Cerjan, D. Kosloff, R. Kosloff, and M. Reshef, "A nonreflecting boundary condition for discrete acoustic and elastic wave equations," *Geophysics*, vol. 50, pp. 705–708, 1985.
13. R. Kosloff and D. Kosloff, "Absorbing boundaries for wave propagation problems," *J. Computational Physics*, vol. 63, pp. 363–376, 1986.
14. C. M. Rappaport and L. Bahrmasel, "An absorbing boundary condition based on anechoic absorber for EM scattering computation," *J. Electromag. Waves Appl.*, vol. 6, no. 12, pp. 1621–1634, 1992.
15. J.-P. Berenger, "A Perfectly Matched Layer for the Absorption of Electromagnetic Waves," *J. Comput. Phys.*, to be published.

Received 3-24-94

Microwave and Optical Technology Letters, 7/13, 599–604

CCC 0895-2477/94

A NEW BROADBAND CIRCULAR PATCH ANTENNA

Supriyo Dey, C. K. Aanandan, P. Mohanan, and K. G. Nair
Department of Electronics
Cochin University of Science & Technology
Kochi 682 022, India

KEY TERMS

Antenna, circular patch, broadband

ABSTRACT

A simple technique to improve the impedance bandwidth of a circular microstrip patch antenna using two sectoral slots is proposed. Using this design more than 5% impedance bandwidth is obtained. The added advantage of this new antenna is that it can be fed by a 50-Ω microstrip line. © *1994 John Wiley & Sons, Inc.*

INTRODUCTION

Microstrip antennas are quickly replacing conventional antennas due to advantages such as light weight, small size, low production cost, and conformal nature. The commonly used radiating elements are rectangular and circular patches. The inherent disadvantage of these antennas is their extremely narrow impedance bandwidth. Although numerous methods are described in the literature to improve the impedance bandwidth of rectangular patch antennas [1–4], only a few techniques are available on bandwidth enhancement of a circular microstrip patch. This is mainly due to the limited use of the circular patch antenna because of high input impedance along its circumference, which restricts the direct use of a 50-Ω microstrip line as feed. A method to overcome this constraint has already been proposed by the authors, wherein, a sectoral slot shunted with a conducting strip is made on the patch [5]. This antenna shows wide variation in input impedance along the circumference and thus can easily be matched with a microstrip line of any impedance.

One of the techniques commonly used to enhance the bandwidth of the circular patch is by using a parasitic element over the patch in a stacked fashion [6]. Another conventional method is the use of a thick dielectric substrate to improve the impedance bandwidth of the circular patch antenna [7]. Even though there is substantial improvement in the impedance bandwidth of the antennas, in both cases the structure becomes bulky and complex. In this article we report a new technique to enhance the impedance bandwidth of circular patch antenna on thin dielectric substrates.

DESIGN AND EXPERIMENTAL DETAILS

The schematic diagram of the antenna is shown in Figure 1. Two sectoral slots are made on the patch surface. The presence of the sectoral slots on the patch causes the antenna to resonate at two adjacent frequencies, which results in the enhancement of the impedance bandwidth.

As a typical example, an antenna is fabricated on a dielectric substrate having thickness $h = 0.16$ cm and dielectric constant $\epsilon_r = 4.5$. The radius r of the patch is 4.95 cm and the sectoral slot angle θ is 6°. The angular position of the 50-Ω feed point from the center of the sectoral slot ϕ is 30°.

The VSWR plot of the antenna is shown in Figure 2. The 2:1 VSWR bandwidth of the antenna is 47.66 MHz and the central frequency is at 882.7 MHz. This corresponds to a 5.4% impedance bandwidth. This is much larger than the impedance bandwidth of 1% to 2% of ordinary circular patch antennas.

The E- and H-plane radiation patterns of the antenna at the central frequency and the two end frequencies (normal-

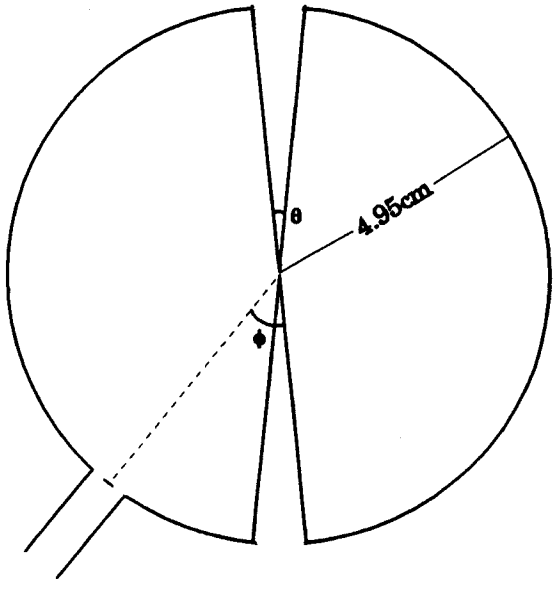

Figure 1 Schematic diagram of the antenna